

PROCEEDINGS OF SPIE

[SPIDigitalLibrary.org/conference-proceedings-of-spie](https://spiedigitallibrary.org/conference-proceedings-of-spie)

Confocal microscopy for high-precision non-contact optical measurements

Micah A. Johnson, Charles C. Kankelborg, Rubin Meuchel, Roy Smart

Micah A. Johnson, Charles C. Kankelborg, Rubin Meuchel, Roy Smart, "Confocal microscopy for high-precision non-contact optical measurements," Proc. SPIE 10747, Optical System Alignment, Tolerancing, and Verification XII, 107470A (19 September 2018); doi: 10.1117/12.2319597

SPIE.

Event: SPIE Optical Engineering + Applications, 2018, San Diego, California, United States

Confocal microscopy for high-precision non-contact optical measurements

Micah A. Johnson^a, Charles C. Kankelborg, Rubin Meuchel, and Roy Smart

^aMontana State University, Bozeman, United States

ABSTRACT

The EUV Snapshot Imaging Spectrograph (ESIS) is a slitless, tomographic imaging spectrograph for observing the solar transition region in extreme ultraviolet (EUV) at 63 nm wavelength. An array of concave diffraction gratings re-image from the telescope prime focus to our CCD detectors. The instrument is aligned and focused in visible light, using substitute diffraction gratings ruled for the red HeNe laser line. To transfer precise alignment and focus of the visible gratings to the EUV gratings, we have developed a miniatuized, three point, non-contact measurement system, TEA (Transfer ESIS Alignment). TEA locates the grating surface using confocal microscopy, with three independent channels scanned together on a single stage, to specify the position and orientation of the spherical surface. Challenges for this measurement include the small size of the ESIS gratings ($\sim 16 \times 20$ mm), their curved surfaces, diffraction effects, the alignment of tiny optics within TEA, and the mechanics used to repeatably mount the gratings. Our testing shows that the intrinsic repeatability of our measurement apparatus is approximately $2 \mu\text{m}$. In practice, however, our error is dominated by the process of mounting the grating subsystem in TEA, which introduces $12 \mu\text{m}$ differences between subsequent runs. This level of repeatability meets our requirements for ESIS.

Keywords: Confocal Microscopy, Optical Tooling, Metrology, Surface Measurement, Optical Transfer, Diffraction, Extreme Ultraviolet, Imaging Spectrograph, Computed Tomography Imaging Spectroscopy

1. INTRODUCTION

In February of 2005, and again in August 2015, the Multi-Order Solar EUV Spectrograph (MOSES)^{1,2} was launched on a sounding rocket to an altitude of ~ 300 km, where solar extreme ultraviolet (EUV) radiation from the sun suffers practically no attenuation. MOSES is a new type of spectrograph that allowed for the imaging of the solar transition region with a multilayer coated, concave diffraction grating, in multiple diffraction orders. The operating principle of the spectrograph is similar to computed tomography imaging spectroscopy (CTIS),³⁻⁵ except that in this case, the objective is to resolve the profile of a strong spectral emission line. The multiple narrow band images are dominated by a single spectral line. Imaging in multiple spectroscopic orders allows for a tomographic reconstruction of the spectral line profile at every point in a wide, two dimensional field of view.^{2,6-8} Now, a successor of MOSES, the EUV Snapshot Imaging System (ESIS), is scheduled for launch in the summer of 2019. ESIS contains diffraction gratings ruled for EUV light in first order, and their alignment to our CCD detectors is critical. As a first step in this process, the instrument is built up and aligned using a red HeNe laser source and a set of “visible alignment gratings” (VIS). The position and orientation of the visible alignment gratings is recorded using confocal microscopy, and then transferred to the EUV gratings. The confocal microscopy system, associated tooling, and mounting fixtures make up an instrument called TEA (Transfer ESIS Alignment), and is the main topic of this paper.

Further author information: (Send correspondence to M.A.J)

M.A.J.: E-mail: jamljohnson09@gmail.com, Telephone: 208 794 7903

C.C.K.: E-mail: kankel@montana.edu, Telephone: 406 994 7853

R.M.: E-mail: rubin.meuchel@montana.edu

R.S.: E-mail: roytsmart@gmail.com

1.1 ESIS

A forthcoming paper by Courrier et al. (*in preparation for JATIS*) will describe the ESIS instrument in detail; for now, we summarize the instrument in sufficient detail to motivate the present paper on alignment transfer from the visible alignment gratings to the flight ultraviolet gratings. ESIS uses a novel optical design for the tomographic imaging of spectral line profiles as a function of skyplane position, for the strong 63 nm line of O V. Figure 1 shows an optical schematic of ESIS. Sunlight comes into ESIS, and is brought to focus at a field stop by a ~ 150 mm diameter parabolic primary mirror with 1 m focal length. After passing through the field stop, the diverging light encounters a radially symmetric array of concave diffraction gratings. Each grating re-images, at $4\times$ magnification, from the prime focus to a corresponding CCD camera, located off axis just outside and behind the perimeter of the primary mirror. ESIS will use four of six available grating positions for the first flight. The flight gratings have groove spacings and multilayer coatings specified for imaging the O V spectral line at 63 nm. A spherical variable line space design is used to correct aberrations.^{9,10}

ESIS images will combine spectral and spatial information in an interesting way. Since there is no slit, both the source position and the wavelength affect where a photon lands on the imaging detector. Our first generation instrument, MOSES, has similar properties, except that the MOSES images are different spectral orders of a single diffraction grating rather than different dispersion angles of multiple gratings. Based on our prior experience with the MOSES instrument, fruitful methods of analysis will range from manual or automated techniques to extract doppler shifts^{8,11} to full tomographic reconstructions of the spectra.^{1,2,7}

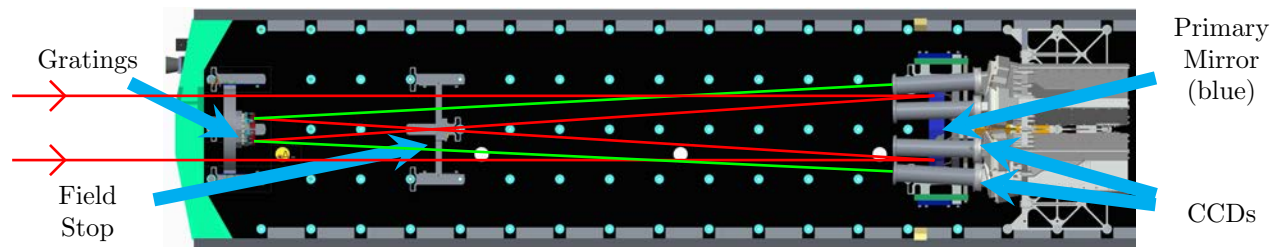


Figure 1. Solid model of ESIS with ray paths and major components indicated.

1.2 Motivation and Theory of ESIS Alignment

Direct alignment of the EUV diffraction gratings would have to be done under vacuum with a collimated 63 nm line source of arc second quality. This would be inordinately time consuming and expensive. Instead, as an intermediary step, we will align and focus the system using the VIS gratings in place of the EUV gratings. Our light source is a spherical wave interferometer fed by a HeNe laser (632.8 nm). The beam is collimated using a high quality telescope. The focus of this system is set by inserting a reference flat and nulling the fringes. Once the collimated beam is aligned to the axis of the ESIS telescope, we install and align the VIS gratings. Once the VIS gratings are aligned and the system is focused from end to end, the position on three points on the surface of each grating are recorded using TEA. The EUV gratings are then mounted and measured using TEA, and shimmed to reproduce the exact alignment of the VIS gratings. In practice, a small complication arises because of manufacturing variations. Each grating has a slightly different radius of curvature, which we have measured interferometrically. Small corrections are made during alignment transfer to compensate for this.

The grating array used in ESIS is mounted to a plate called the tuffet. There are two tuffets. One tuffet holds the VIS gratings, and the other EUV gratings. The VIS tuffet is used for alignment in ESIS, and the EUV tuffet is used for flight after alignment has been transferred from the VIS to EUV gratings. The use of one tuffet for the VIS gratings and another for the EUV gratings has several important implications:

1. The alignment and focus of the VIS gratings are effectively preserved, so long as the parts assembled the tuffet are not loosened.
2. The VIS alignment only has to be done once. It can be restored easily by mounting the VIS tuffet to ESIS.

3. Hence, we can verify at will that no other parts of the ESIS instrument have shifted. This is particularly important before and after operations involving mechanical shock and vibration such as shipping, shake testing, and launch.
4. The EUV alignment, performed using TEA, is likewise preserved. EUV and VIS tuffets can be compared at any time using the TEA to ensure that they agree.
5. Since the tuffets preserve alignment states, the TEA can be viewed simply as a comparator. It requires no absolute calibration, but must hold its zero and make accurate *relative* position measurements.

1.3 Confocal Microscopy

Confocal laser scanning microscopy uses light to perform a series of distance measurements. Generally, confocal microscopes bring light to a focus on an object near the focus. The amount of light that returns through the microscope to a beamsplitter near the light source is maximized when the surface of the sample is at the focus. By scanning the confocal microscope system along the focus direction and recording a series of return intensities, it is possible to determine the exact location of the sample surface.¹² For the grating alignment transfer, as discussed in the previous section (1.2), we are interested in knowing the position of the gratings at three points. For this purpose, we have developed the three-channel scanning confocal microscope system of TEA.

The paper will first discuss the optical design of TEA, and how it uses confocal microscopy for the transferring of alignment from VIS to EUV gratings. Once the optical design is understood, the mechanical design is shown. To detect the light reflected off the gratings, photodiodes were used, so their circuitry is also discussed. Software and data analysis developed for the control of TEA is then presented. Finally, we present results of precision and repeatability of the subsystems within TEA, and testing data that assess the thermal stability of the apparatus.

2. DESIGN

2.1 Optical Design

Within the measurement head of TEA, there are three identical confocal microscopes. The schematic design of a single microscope is shown in Figure 2. Each microscope uses a 4.5 mW, 635 nm solid state laser diode module with elliptical beam of 3.8 mm × 1.2 mm. The laser is mounted into a part that allows for mechanical shimming to adjust the tip/tilt of the laser. We shim the laser to produce a symmetric beam at the outset of the condenser pair shown in Figure 2. To reduce the aberrations introduced by measuring a non-flat grating, and to underfill the lens train so that the system is less sensitive to the tip/tilt of the target, a small baffle with a circular aperture of 0.78 mm is used to stop down the laser beam. Light then passes through a beamsplitter, which reflects half the light onto a black anodized beam stop (not shown), and the remainder continues undeviated.

The light transmitted by the beamsplitter is focused by a cylindrical gradient refractive index (GRIN) lens. The GRIN lens was selected for its small size (\varnothing 2 mm × 5 mm) and relative ease of alignment. Light diverges from the focal point on the exit surface of the lens. A symmetric condenser pair re-images light from the GRIN lens focus to the sample, without magnification. Reflected light re-enters the condenser pair, and proceeds through

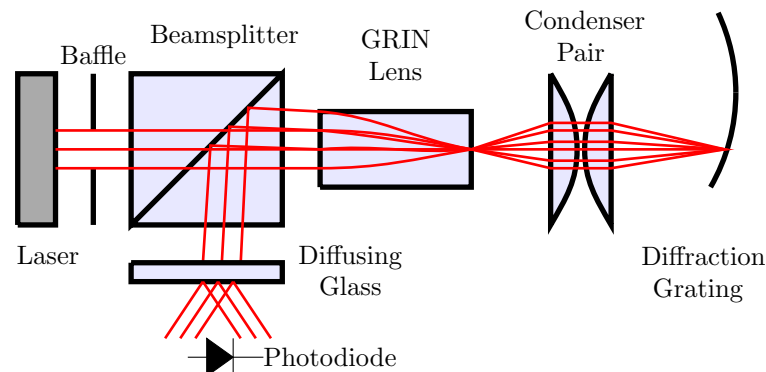


Figure 2. Ray trace illustration of one of the three microscopes withing the TEA measurement head.

the GRIN lens. Half the beam is diverted by the beamsplitter to a piece of diffusing glass, where a photodiode measures the returned signal.

An ESIS grating is placed in front of the measurement head such that all three microscopes can focus on the surface of a single grating. The measurement head is scanned to find the grating surface at three points. This is a relative measurement, in the sense that the only meaningful “zero” is the position of a properly aligned VIS grating. Since the grating is concave, and since the three confocal microscopes are aligned to the same axis, each of the three measurement heads “sees” a tilted surface. Light reflected off the grating is returned back through the measurement head, but at an angle. Because the condensers are much larger than the beam size, the return beam is not vignettted when the grating is at focus. The diffusing glass serves to reduce the sensitivity of the system to beam offset resulting from tilt of the sample (grating), and to remove any diffraction effects that may influence the intensity of light on the photodiode.

2.2 Mechanical Design

Two major components of TEA, the measurement head (Figure 3) and the grating fixture (Figure 4), are custom mechanical designs which we describe in this section.

2.2.1 Measurement head

The measurement head holds three confocal microscopes in a triangular configuration, all within a cross-sectional area less than 200 mm². The small size is needed so all three of the microscopes within the measurement head can simultaneously focus on the surface of the grating under test.

To best describe the mechanical design and components within the measurement head, numbers listed will refer to parts of the solid model shown in Figure 3. The lasers (1) are held in individual “convection mounts” (2) using set screws. Since the lasers dissipate power and tend to heat the apparatus, the convection mounts feature deeply milled slots to facilitate convection cooling. Each of the three convection mounts are held in place on a single interface plate (3) using three screws each, so that each convection mount can be shimmed independently to adjust the tip/tilt of the lasers. The measurement head is built around a T-block (4) which holds all the fixtures for mounting the optics. The interface plate connects to one end of the T-block, thereby fixing the lasers to the rest of the optical system.

Each channel has its own photodiode, epoxied onto a fixture (5), in a housing (6). The diffusing glass (between 6 and 7) is sandwiched between the photodiode housing and the beamsplitter mount (7). The beamsplitter mount holds the beamsplitter in place on the T-beam, and holds the beam stop (between 3 and 7).

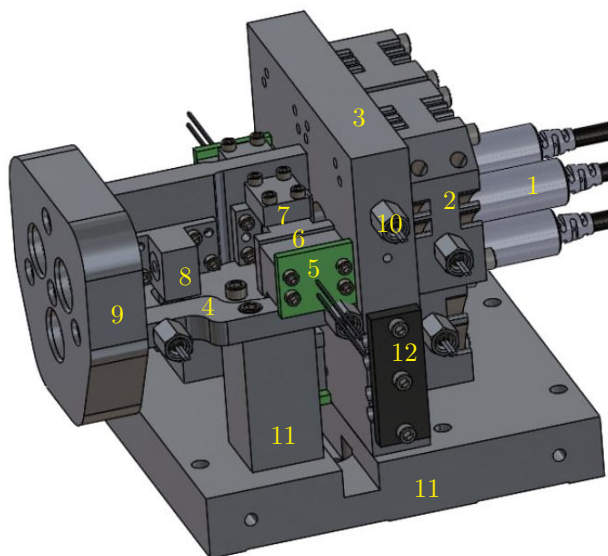


Figure 3. Solid model of TEA measurement head. Numbers referred to throughout Section 2.2

The GRIN lens also mounts to the T-block using a simple static mount (8) with an epoxy injection hole for securing the lens. Finally, on the other end of the T-block from the laser interface plate is a mount that holds the condenser lens pairs (9). The holes in the lens mount are threaded to allow the condenser pair to be held in place with retaining rings. Additionally, there are multiple tapped holes in the measurement head for attaching thermistors (10) mounting structures (11), and wire clamps for strain relief (12).

2.2.2 Grating fixture

The complete TEA optomechanical apparatus is shown in Figure 4, with gratings mounted. On the left side are the measurement head (13), an automated stage (14), and a manual stage (15). The manual stage extends the range of motion so that the automated stage cannot make contact with the gratings under test. Once in position, repeatability is ensured by staking the manual stage in place once set to a position where the automated stage cannot run into the gratings under test. On the right side are the gratings (16), which are attached by semi-rigid hexapod mounts to their base plates. The base plates are shimmed and mounted to the “tuffet” (17) via spherical washer sets to ensure consistent bolt-up. The gratings, base plates, and tuffet are part of the ESIS instrument. On the flight grating fixture, two pins and three finely machined shims ensure a repeatable mechanical interface. On TEA, the tuffet interfaces by identical means to a rotating mount (18). The rotating mount can be rotated about a precision shoulder screw at the center of the grating array. It is pinned to the angled support (19) in such a way that it can be rotated with precise repeatability to place each of the gratings opposite the measurement head, while holding the baseplate of the the grating under test orthogonal to the measurement head scanning direction. All of the parts of TEA are securely bolted to an custom plate with thermistor inserts.

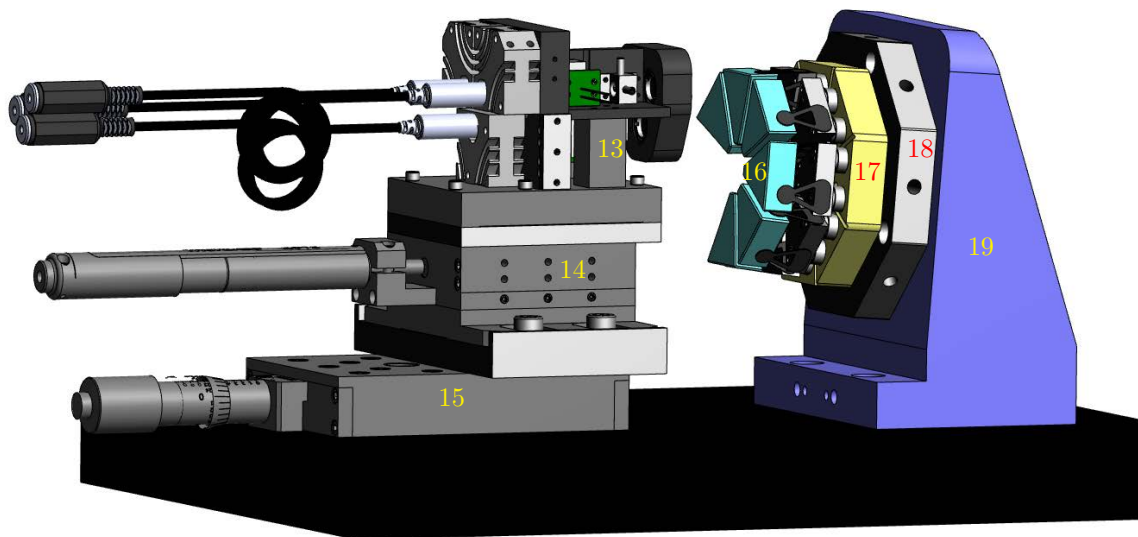


Figure 4. Solid model of TEA: the mounted measurement head (left), and grating fixture (right). The measurement head rests on a stage assembly (14-15) that facilitates scanning for the grating position measurement.

2.3 Electrical Design

An electrical block diagram of TEA is shown in Figure 5. The computer runs the automated stage controller to scan the measurement head. The current from the photodiodes in the measurement head is converted to a voltage in the transimpedance amplifier, which is described in Section 2.3.1. The resistance of each thermistor is scaled by a voltage divider. The resulting voltages are measured and digitized by the voltmeter, and acquired as digital data by the computer. The input impedance of the voltmeter is $1\text{ M}\Omega \pm 2\%$, which is high enough that buffering was not required for the output filter of the transimpedance amplifier, nor for the thermistor voltage dividers.

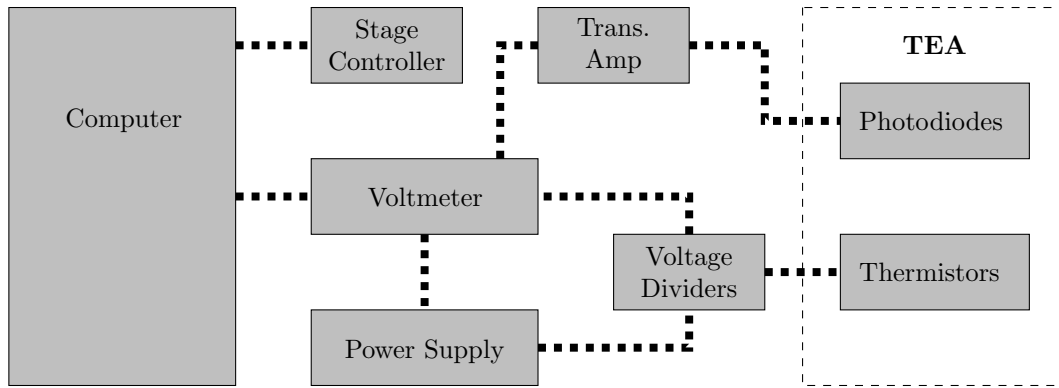


Figure 5. Electrical block diagram for TEA control and data collection.

2.3.1 Transimpedance amplifier

TEA uses three photodiodes, one for each channel within the measurement head. An individual photodiode circuit consists of a transimpedance amplifier in series with a low-pass filter as shown in Figure 6. The transimpedance amplifier converts the current response from the photodiode into voltage. The low pass filter suppresses noise above 8 Hz. The measurement frequency is 2-5 Hz depending on the voltage. Each of the three circuits used their own 9 V battery source. Batteries were used for their low noise as opposed to a lab power supply. The batteries are replaced before every measurement run to ensure that they are fully charged.

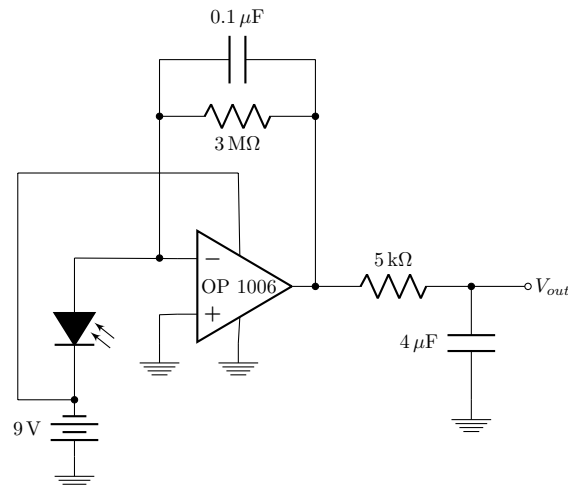


Figure 6. Transimpedance amplifier used for preparing photodiode signal for measurement.

2.3.2 Temperature monitoring

The temperature fluctuations due to laser warm up and the building central air system have the potential to cause thermal expansion within TEA, reducing the repeatability of the instrument. The temperature monitoring system allows us to obtain a detailed record of the TEA thermal state throughout the measurement, so that we can ensure that an accurate comparison is made between the VIS and EUV gratings.

The temperature on TEA was monitored using 9 thermistors epoxied into various parts of the measurement head and grating fixtures. The thermistors are all nominally 5000 kΩ. We use 4990 kΩ ± 1% precision resistors in series with them to produce output voltages. All voltage dividers used the same lab power supply and ground. Analysis of the temperature gathered from the thermistor circuits can be found in Section 2.4.2 and 3.2.

2.4 Software Design

Thousands of data points are required to know the position of max intensity to an adequate tolerance. To gather all the data, we developed a software for gathering and analyzing data. Software was primarily developed in Python 3.5 and Matlab. For a general overview of the software see the block diagram shown in Figure 7. The software is split up into two main components: control and analysis. Python is used for control, and communicates with the stepper motor and voltmeter. Once control system gathers all the data, Matlab analyses it. The analysis part of the software decides whether more data is needed, or how precisely the positions of max intensity is known.

2.4.1 Control software

The control software is responsible for moving the motor, measuring voltage, and logging data. Refer to the blue box in Figure 7 for a block diagram of the control software. To initialize the software, initial conditions can put into Python before executing the main script. The initial conditions that could be specified are the start position, end position, number of times to measure each position, the distance between each step to measure, the type of grating, and the serial number of the grating. Once initialized, the program can be run. Python moves the motor to the start position, takes measurements from all channels of the voltmeter, interprets the temperature voltages into units of °C via the Steinhart-Hart equation, and repeats until getting to the end position. Once at the end position, the motor loops back to the start position and repeats the measurements. We chose to have the motor loop back to the start position, rather than take many measurements at a position at once, because any long term drifts in the system would be apparent in the more data. The motor continues to

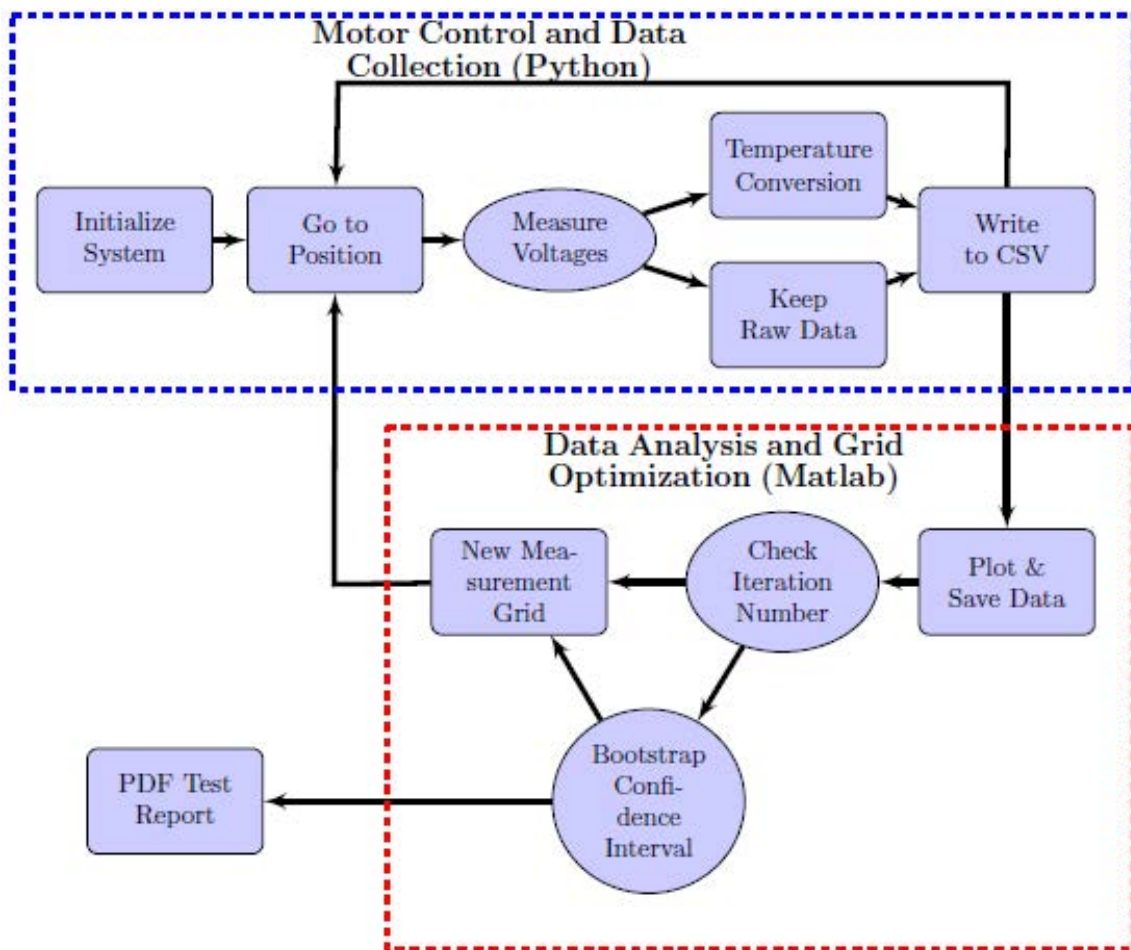


Figure 7. Block diagram of software used to run TEA.

loop back the number of times specified in the initial conditions as the number of times to measure each position. Once all the data is collected and saved to a file, Python opens Matlab where the data is analyzed.

2.4.2 Analysis Software

Matlab analyzes the data gathered by the control software. For a more visual depiction, refer to the red box in Figure 7. It first plots the temperature data over the course of the experiment. It then formats the photodiode data such that voltages collected at identical positions over different scans can be referenced together. It averages voltages collected at identical positions, and fits the averaged data to a fourth degree polynomial. It then plots the data with the fits. The analysis software then creates new initial conditions for the control software based on a constant offset from the positions of peak intensity. The new initial conditions are optimized to take as few measurements as possible, while still getting enough information to precisely know the positions of peak intensity in all three channels, thus reducing the amount of time required for a test.

The cycle of the control software calling the analysis software for new initial conditions happens several times until a large enough amount of data is gathered. Once enough data is gathered, the analysis software computes how precisely the positions of peak intensity are known with bootstrapping. It is possible to estimate a confidence interval for the peak positions. The software randomly samples with replacement intensity measurements from each position within the scan. It averages re-sampled data that occurs at the same positions, and fits the averaged data to a fourth degree polynomial. This re-sampling technique is repeated 10000 times, producing a distribution of “guesses” for the positions of max intensity. Each channel has its own distribution of “guesses” from which it calculates a confidence interval. From the distribution, the software calculates a 98% confidence interval. The test report contains the position that was seen most often in the bootstrapping, along with the uncertainty described by the confidence interval for each channel.

3. DATA ANALYSIS

3.1 Photodiode Analysis

A description of how data is analyzed within the software can be found in Section 2.4.2. Here instead, we discuss trends in the data across multiple measurements. As referenced in previous sections, each of the three channels in the measurement head contain a photodiode, which outputs a signal proportional to the intensity of light reflected by the gratings. An example of such data can be seen in Figure 8. An example of a distribution of the position of peak intensity from the bootstrapping algorithm for a single channel can be seen in Figure 9.

Note the strange spatial noise in the intensity curves in Figure 8. Figure 8 is created by scanning over the same positions 20 times over the course of roughly 6 hours. Because of this large sample size and good repeatability,

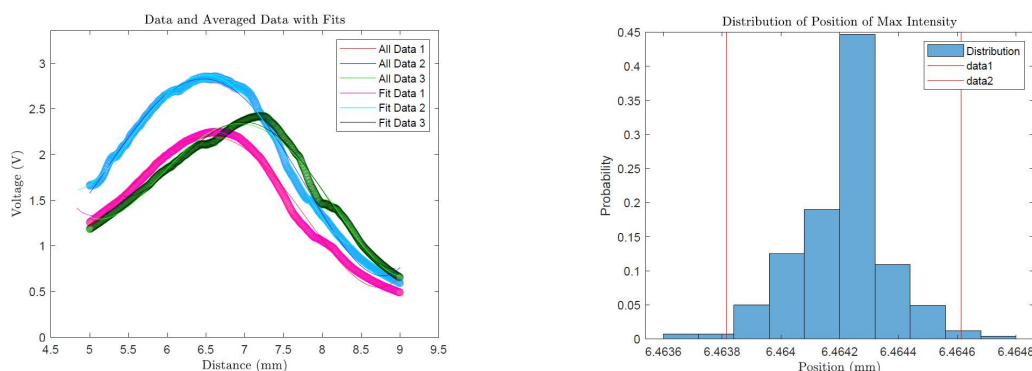


Figure 8. Example of data gathered from TEA when measuring Figure 9. Example distribution of position of max intensity found the position of a grating. The width of a curve at a position is through bootstrapping. Red lines represent edges of the 98% proportional to the uncertainty in the intensity at that point. confidence interval.

we can know the deviations from a 4th order polynomial are physical, and not the result of an anomaly in the system. Factors like temperature change, fluctuations in power source, and diffraction are all controlled, so any deviations from ideal data must be due to the physical characteristics of the TEA system. Major deviations occur at ~ 5.8 mm in blue, 6.5 mm in black, and 7.9 mm in red. These deviations were not present in the early development of TEA, so are due to testing a curved surface rather than a flat one.

The lines seen in Figure 8 show the 4th order polynomial fit to the data. While it does not appear that the fits will accurately represent the peak intensity, this does not matter. Only the repeatability of where the fit calculates the peaks to be located matters. Perhaps a more sophisticated model fit to the data would increase repeatability, but would also likely take longer in software as the fit must be performed thousands of times in the bootstrapping process as described in Section 2.4.2.

3.1.1 Tests for repeatability

To measure the repeatability of TEA and the subsystems within, we report the standard deviation of the differences between measurements that should yield the same output. This approach allows for describing the repeatability across all channels of TEA. For example, say three measurements are run on a grating giving results of channel #1: 4.002, 4.005, 4.023, channel #2: 5.334, 5.333, 5.322, channel #3: 8.892, 8.871, 8.900. The three positions measured for channel #1 are subtracted from one another, and the same for the other channels, giving a distribution of differences of 0.003, 0.021, 0.018, 0.001, 0.011, 0.012, 0.008, 0.029, 0.021. The standard deviation of this distribution is calculated to be .008, and this number we would be report as the repeatability.

Tests were performed to isolate the magnitude of error introduced by different parts of TEA. When running a test, 10-20 measurements are taken at every position. With the bootstrapping algorithm, the position of peak intensity is known to $\sim 0.3 \mu\text{m}$ for a single test. This number does not capture all the relevant uncertainties, as we are interested in the differences between gratings. If multiple tests are run on a single grating without changing anything, TEA outputs results consistent to $\sim 2 \mu\text{m}$. This is the repeatability of the measurement head.

In an effort to make the mounting of the gratings repeatable, we used pins, precision shoulder screws, three-point contacts, and other techniques described in Section 2.2. Procedurally, the experiment is performed in a class 1000 clean tent, mating surfaces are inspected and cleaned before each bolt up, and consistent torques are used to maximize repeatability. The tuffet can be rotated about its center by moving the rotation mount on the angle plate, and this is done to change which gratings is being scanned by the measurement head. By rotating the tuffet back and forth between two gratings, and taking measurements of each, we found the rotation had a repeatability of $\sim 8 \mu\text{m}$. Finally, the largest source of error was introduced by the removal of the tuffet from the grating structure. When switching from the tuffet containing VIS gratings to the tuffet with the flight gratings, the fixtures that hold the tuffet and gratings have to be disassembled. When this is done, an error of $\sim 12 \mu\text{m}$ is introduced. So, while the measurement head of TEA has great repeatability on the micron level, the mounting structures for the gratings have an error an order of magnitude larger. Fortunately, this level of repeatability is acceptable for ESIS.

3.2 Temperature Analysis

Early tests with TEA showed that the temperature tended to drift by a few degrees over the course of a single test. TEA is made primarily of aluminum. A quick calculation shows that a 1°C change on a nominal 4 cm length of the TEA T-bar produces a length change of nearly 1 μm . Accordingly, we decided to monitor the temperature of the apparatus carefully, and to take the necessary measures to keep the temperature stable within $\pm 1^\circ\text{C}$. We note that with these measures in place, TEA has achieved $\sim 2 \mu\text{m}$ repeatability from run to run on a single grating. Hence, the experimental procedures described below have reduced thermal fluctuations to the point where they do not dominate the repeatability of the measurement head.

To improve the thermal stability of TEA, we enclosed the instrument in a styrofoam box. We performed a 16 hour test collecting temperature from 9 thermistors on TEA while it was in the box. Results can be seen in Figure 10.

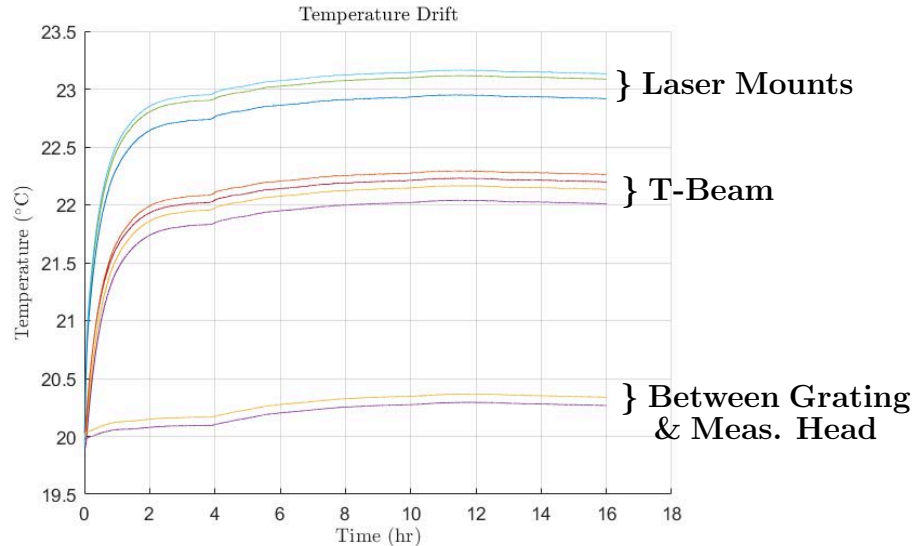


Figure 10. Temperature characterization of TEA over 16 hours. Annotations refer to where thermistors were mounted on TEA.

Note the large transient in temperature during the first hour. This is the initial warm up after turning the lasers on at the beginning of the test. After an hour, the temperature stops fluctuating by more than a degree. Consequently, our procedure allows one hour after turn on for the instrument to warm up.

Note the gradual temperature increase of approximately 0.2°C in all channels, starting at 4 hours into the test. This may be due to the building air conditioning turning off at the end of the day.

Finally, note the three distinct groups. There are three channels at the highest temperature. These channels were connected to the convection laser mounts. As the lasers are the main source of heat, it makes sense that three of the channels are warmer than the others. The group of four come from thermistors attached to the T-beam. While somewhat isolated from the lasers, the T-beam only has approximately a centimeter between it and the lasers. The lower two channels had thermistors on a plate between the grating mount and the measurement head stack. These channels are almost entirely isolated from lasers. The small temperature changes present in the lower two channels are not intrinsically worrisome, but the temperature difference between this outer structure and the T-Beam is what must be kept constant in time so as to avoid thermal movement of the measurement head relative to the gratings.

Temperature is monitored during every test to ensure that TEA is in thermal equilibrium while taking measurements, improving repeatability. A graph similar to Figure 10 is produced for every test, though it rarely shows more than a 1°C of fluctuation in any channel. Most importantly, the temperatures during the VIS grating measurement must be close enough those during the EUV grating measurement. This is necessary to ensure an accurate comparison. Our experience so far indicates that this should not be difficult.

4. CONCLUSIONS

We have described a measurement approach that allows us to align an EUV spectrograph in visible light, then transfer that alignment from visible (VIS) gratings to EUV gratings. Our approach uses a unique, three channel confocal microscope measurement head to record the positions of the VIS gratings, and transfer the alignment precisely to the EUV gratings. While coordinate measuring machines and non-contact measurements using a variety of techniques have been in use in optical applications for many years, We anticipate that our alignment transfer technique may have other applications in research and industry.

The high precision, minimal optics, small size, and little internal alignment necessary make the alignment transfer instrument (TEA) unique. The measurement head can repeatably determine the orientation of a mirror or grating to $2\ \mu\text{m}$. The fixtures for holding the optics under test are less repeatable at $12\ \mu\text{m}$, but this could be

improved with more precise machining, bolt up, and temperature control. With this level of precision, we are able to repeatably transfer alignment from our set of VIS to EUV gratings, obviating the need for alignment and focus in vacuum.

ACKNOWLEDGMENTS

This work is supported the NASA Sounding Rocket Program, Grant NNX14AK71G, and the Undergraduate Scholars Program at Montana State University.

Special thanks to Jacob Parker, Kevin Zach, and the rest of the ESIS team for their help in the development of TEA.

REFERENCES

1. J. L. Fox, *Snapshot imaging spectroscopy of the solar transition region: The Multi-Order Solar EUV Spectrograph (MOSES) sounding rocket mission*. PhD thesis, Montana State University, 2011.
2. T. L. Rust, *Explosive Events in the Quiet Sun: Extreme Ultraviolet Imaging Spectroscopy Instrumentation and Observations*. PhD thesis, Montana State University, Bozeman, MT, July 2017.
3. T. Okamoto and I. Yamaguchi, "Simultaneous acquisition of spectral image information," *Opt. Lett.* **16**, pp. 1277–1279, Aug 1991.
4. M. Descour and E. Dereniak, "Computed-tomography imaging spectrometer: experimental calibration and reconstruction results," *Appl. Opt.* **34**, pp. 4817–4826, Aug 1995.
5. C. DeForest, D. F. Elmore, M. P. Bradford, J. Elrod, and D. L. Gilliam, "Stereoscopic spectroscopy for efficient spectral imaging and magnetography," *The Astrophysical Journal* **616**(1), p. 600, 2004.
6. C. C. Kankelborg and R. J. Thomas, "Simultaneous imaging and spectroscopy of the solar atmosphere: advantages and challenges of a 3-order slitless spectrograph," in *UV/EUV and Visible Space Instrumentation for Astronomy and Solar Physics*, O. H. Siegmund, S. Fineschi, and M. A. Gummin, eds., **4498**, pp. 16–26, Dec. 2001.
7. J. L. Fox, C. C. Kankelborg, and T. R. Metcalf, "Data inversion for the Multi-Order Solar Extreme-Ultraviolet Spectrograph," in *Optical Spectroscopic Techniques and Instrumentation for Atmospheric and Space Research V*, A. M. Larar, J. A. Shaw, and Z. Sun, eds., **5157**, pp. 124–132, Nov. 2003.
8. J. L. Fox, C. C. Kankelborg, and R. J. Thomas, "A Transition Region Explosive Event Observed in He II with the MOSES Sounding Rocket," **719**, pp. 1132–1143, Aug. 2010.
9. T. Harada and T. Kita, "Mechanically ruled aberration-corrected concave gratings," *Appl. Opt.* **19**, pp. 3987–3993, Dec 1980.
10. K. Middleton, V. Da Deppo, L. Poletto, U. Schühle, R. J. Thomas, and P. R. Young, "Optical Design Of The Extreme Ultraviolet Spectrometer (EUS) On Board Solar Orbiter," in *Second Solar Orbiter Workshop, ESA Special Publication* **641**, p. 48, Jan. 2007.
11. H. T. Courier and C. C. Kankelborg, "Using local correlation tracking to recover solar spectral information from a slitless spectrograph," **4**, p. 018001, Jan. 2018.
12. G. Berkovic and E. Shafir, "Optical methods for distance and displacement measurements," *Adv. Opt. Photon.* **4**, pp. 441–471, Dec 2012.